



This discussion paper is/has been under review for the journal Atmospheric Chemistry and Physics (ACP). Please refer to the corresponding final paper in ACP if available.

# On the potential of ICOS atmospheric CO<sub>2</sub> measurement network for the estimation of the biogenic CO<sub>2</sub> budget of Europe

N. Kadygrov<sup>1</sup>, G. Broquet<sup>1</sup>, F. Chevallier<sup>1</sup>, L. Rivier<sup>1</sup>, C. Gerbig<sup>2</sup>, and P. Ciais<sup>1</sup>

<sup>1</sup>Laboratoire des Sciences du Climat et de l'Environnement, CEA-CNRS-UVSQ, 91191, Gif sur Yvette CEDEX, France

<sup>2</sup>Max Planck Institute for Biogeochemistry, Jena, Germany

Received: 8 December 2014 – Accepted: 27 April 2015 – Published: 20 May 2015

Correspondence to: N. Kadygrov (kadygrov@gmail.com)

Published by Copernicus Publications on behalf of the European Geosciences Union.

On the potential of  
ICOS atmospheric  
CO<sub>2</sub> measurement  
network

N. Kadygrov et al.

Title Page

Abstract

Introduction

Conclusions

References

Tables

Figures



Back

Close

Full Screen / Esc

Printer-friendly Version

Interactive Discussion



## Abstract

We present a performance assessment of the European Integrated Carbon Observing System (ICOS) atmospheric network for constraining European biogenic CO<sub>2</sub> fluxes (hereafter Net Ecosystem Exchange, NEE). The performance of the network is assessed in terms of uncertainty in the fluxes using a state-of-the-art mesoscale atmospheric inversion system assimilating hourly averages of atmospheric data to solve for NEE at 6 h and 0.5° resolution. The performance of the ICOS atmospheric network is also assessed in terms of uncertainty reduction compared to typical uncertainties in the flux estimates from ecosystem models that are used as prior information by the inversion. The uncertainty in inverted fluxes is computed for two typical periods representative of summer and winter conditions in July and in December 2007, respectively. These computations are based on a robust Observing System Simulation Experiments framework. We analyze the uncertainty in two-week mean NEE as a function of the spatial scale, with a focus on the model native grid scale (0.5°), the country scale and the European scale (including western Russia and Turkey). Several network configurations, going from 23 to 66 sites, and different configurations of the prior uncertainties and atmospheric model transport errors are tested in order to assess and compare the improvements that can be expected in the future from (1) the extension of the network, (2) improved prior information or (3) improved transport models. Assimilating data from 23 sites (a network comparable to present day capability) with the estimate of errors from the present prior information and transport models, the uncertainty reduction on two-week mean NEE should range between 20 and 50 % for 0.5° resolution grid cells in the best sampled area encompassing eastern France and western Germany. At the European scale, the prior uncertainty in two-week mean NEE is reduced by 50 % (66 %, down to ~ 43 TgC month<sup>-1</sup> (resp. 26 TgC month<sup>-1</sup>) in July (resp. December). Using a larger network of 66 stations, the prior uncertainty of NEE is reduced by the inversion by 64 % (down to ~ 33 TgC month<sup>-1</sup>) in July and by 79 % (down to ~ 15 TgC month<sup>-1</sup>) in December. When the results are integrated over the well-observed western Euro-

### On the potential of ICOS atmospheric CO<sub>2</sub> measurement network

N. Kadygrov et al.

Title Page

Abstract

Introduction

Conclusions

References

Tables

Figures



Back

Close

Full Screen / Esc

Printer-friendly Version

Interactive Discussion



## On the potential of ICOS atmospheric CO<sub>2</sub> measurement network

N. Kadygrov et al.

Title Page

Abstract

Introduction

Conclusions

References

Tables

Figures



Back

Close

Full Screen / Esc

Printer-friendly Version

Interactive Discussion



pean domain, the uncertainty reduction shows no seasonal contrast. The effect of decreasing the correlation length of the prior uncertainty, or of reducing the transport model errors compared to their present configuration (when conducting real-data inversion cases) can be larger than that of the extension of the measurement network in areas where the 23 stations observation network is the densest. We show that with a configuration of the ICOS atmospheric network containing 66 sites that can be expected on the long-term, the uncertainties in two-week mean NEE will be reduced by up to 50–80 % for countries like Finland, Germany, France and Spain, which could bring a significant improvement of (and at least a high complementarity to) our knowledge about NEE derived from biomass and soil carbon inventories at multi annual scales.

## 1 Introduction

Accurate information about the terrestrial biogenic CO<sub>2</sub> fluxes (hereafter Net Ecosystem Exchange – NEE) is needed at the regional scale to understand the drivers of the carbon cycle. Accounting for the natural fluxes in political agreements regarding the reduction of the CO<sub>2</sub> emissions requires their accurate quantification over administrative areas, and in particular over countries and smaller regional scales at which land management decisions can be implemented.

The atmospheric inversions, which exploit atmospheric CO<sub>2</sub> mole fraction measurements to infer information about surface CO<sub>2</sub> fluxes (Enting, 2002) are expected to deliver robust and objective quantification of NEE at high temporal and spatial resolution over continuous areas and time periods. Global atmospheric inversions have been widely used to document natural carbon sources and sinks (Gurney et al., 2002; Rodenbeck et al., 2003), although the spread of different studies, and thus, likely the uncertainty, remain large at the 1 month and continental scale (Peylin et al., 2013). Such large uncertainties are mainly due to the lack of observations over the continents or to the limited ability of global systems to account for dense observation networks in addition to errors in large-scale atmospheric transport models. However, with an increasing

## On the potential of ICOS atmospheric CO<sub>2</sub> measurement network

N. Kadygrov et al.

Title Page

Abstract

Introduction

Conclusions

References

Tables

Figures



Back

Close

Full Screen / Esc

Printer-friendly Version

Interactive Discussion



number of continuous atmospheric CO<sub>2</sub> observations, primarily in North America and Europe, and with the development of regional inversion systems using high resolution mesoscale atmospheric transport models and solving for NEE at typical resolutions of 10 to 50 km (Lauvaux et al., 2008, 2012; Schuh et al., 2010; Broquet et al., 2011; Meesters et al., 2012), there is an increasing ability to constrain NEE at continental to regional scales.

This paper aims at studying the skill of a regional inversion in Europe, which is equipped with a relatively large number of ground-based atmospheric measurement stations, for estimating NEE at the continental and country scales, down to 0.5° resolution (which is the resolution of the transport model used in the inversion system). It also aims at assessing and comparing the benefits from the measurement network extensions and from future improvement in the inversion system. Such improvement can be anticipated either due to better atmospheric transport models or to the use of better flux estimates as the prior information that gets updated by the inversion based on the assimilation of atmospheric measurements.

Europe is a difficult application area for atmospheric inversion because of the very heterogeneous distribution of vegetation types, land use, and agricultural and industrial activities inside a relatively small domain, and, consequently, because of the need for solving for fluxes at high resolution. Furthermore, its complex terrain also requires a high resolution of the topography when modeling the atmospheric transport (Peters et al., 2010). However, the Integrated Carbon Observing System (ICOS) infrastructure is setting up a dense network of standardized, long-term, continuous and high precision atmospheric and flux measurements in Europe, with the aim of understanding the European carbon balance and monitoring the effectiveness of Greenhouse Gas (GHG) mitigation activities (<http://www.icos-infrastructure.eu/>). The atmospheric network is expected to increase from an initial configuration of around 23 stations (most existing today, hereafter ICOS23) up to around 60 stations in the near future (see ICOS Stakeholder handbook 2013 at [https://www.icos-ri.eu/file/61/download?token=wlyz4g2\\_](https://www.icos-ri.eu/file/61/download?token=wlyz4g2_)).











## On the potential of ICOS atmospheric CO<sub>2</sub> measurement network

N. Kadygrov et al.

Title Page

Abstract

Introduction

Conclusions

References

Tables

Figures

◀

▶

◀

▶

Back

Close

Full Screen / Esc

Printer-friendly Version

Interactive Discussion



stations are relatively far from large urban areas. Therefore, in order to simulate the full amount of CO<sub>2</sub> in the atmosphere, the inversion uses a fixed estimate of the fossil fuel emissions (see below) without attempting at correcting it nor at accounting for uncertainties in these fluxes. The inversion also uses a fixed estimate of the CO<sub>2</sub> boundary conditions at the lateral and top boundaries of the regional modeling domain without attempting at correcting it or at accounting for uncertainties in these conditions. This follows the protocol from Broquet et al. (2011) which assumed that the error from the boundary conditions for the European domain is mainly a bias and which corrects for such a bias in a preliminary step that is independent to the subsequent application of the inversion. In this section we only summarize the main elements of the inversion system, starting with the theoretical framework, while the detailed description can be found in Broquet et al. (2011).

We define the control vector  $\mathbf{x}$  of the atmospheric inversion as the 6 h and 0.5° × 0.5° mean NEE and ocean fluxes. The atmospheric inversion seeks the mean  $\mathbf{x}_a$  and covariance matrix  $\mathbf{A}$  of the normal distribution  $N(\mathbf{x}_a, \mathbf{A})$  of the knowledge on  $\mathbf{x}$  based on (i) the atmospheric transport model, (ii) the prior knowledge  $\mathbf{x}_b$  of  $\mathbf{x}$ , (iii) the hourly mean atmospheric measurements  $\mathbf{y}$ , (iv and v) the covariances  $\mathbf{B}$  and  $\mathbf{R}$  of the distributions of the prior uncertainty and of the observation error assuming that these uncertainties are normal and unbiased (i.e., equal to  $N(0, \mathbf{B})$  and  $N(0, \mathbf{R})$  respectively), and (vi) a Bayesian relationship between these distributions. The observation error is the combination of all sources of misfit between the atmospheric transport model and the concentration measurements other than the prior uncertainty, in particular the measurement errors, the model transport, aggregation and representation errors, and the errors from the model inputs that are not controlled by the inversion.

With this theoretical framework,  $\mathbf{x}_a$  is the minimum of the quadratic cost function  $J(\mathbf{x})$  (Rodgers, 2000):

$$J(\mathbf{x}) = \frac{1}{2}(\mathbf{x} - \mathbf{x}_b)^T \mathbf{B}^{-1} (\mathbf{x} - \mathbf{x}_b) + \frac{1}{2}(H(\mathbf{x}) - \mathbf{y})^T \mathbf{R}^{-1} (H(\mathbf{x}) - \mathbf{y}) \quad (1)$$





of iterations and of inversion experiments. However, it has been checked (see below Sect. 2.2.2) that the convergence is sufficient so that this dependence should not be significant for the quantities of interest.

## 2.2.2 Practical set-up

### 5 Atmospheric transport model

In this study, the operator **H** is based on the CHIMERE mesoscale atmospheric transport model (Schmidt et al., 2001) forced with ECMWF winds. We use a configuration with a  $0.5^\circ \times 0.5^\circ$  horizontal grid and with 25  $\sigma$ -coordinate vertical levels starting from the surface and with a ceiling at  $\sim 500$  hPa. The spatial extent of the corresponding domain is described below in section. CHIMERE is an off-line transport model. Hourly mass-fluxes are provided by the analyses of the European Centre for Medium-Range Weather Forecasts (ECMWF). The relatively high vertical and horizontal resolutions of CHIMERE allow a good vertical discretization of the Planetary Boundary Layer (PBL; the first 14 levels are below 1500 m) along with a good representation of the orography and dynamics to match high frequency observations better than with global configuration whose typical horizontal resolution is  $\sim 3^\circ$  (Peylin et al., 2013).

### Spatial and temporal domains

In this study, we use the European domain shown in Fig. 1a which covers most of the European Union and some of Eastern Europe, with a land surface area of  $6.8 \times 10^6$  km<sup>2</sup>. Its southwest corner is at  $35^\circ$  N and  $15^\circ$  W, and its northeast corner is at  $70^\circ$  N and  $35^\circ$  E. Two temporal windows are considered, from 30 June to 20 July 2007 and from 2 to 22 of December 2007 (of almost three weeks each). The choice of those periods of three weeks is a tradeoff between widening the scope of the study and computational burden. The Monte Carlo-based flux uncertainty reduction calculations require large computing resources, while we test three different network configurations for two differ-

## On the potential of ICOS atmospheric CO<sub>2</sub> measurement network

N. Kadygrov et al.

Title Page

Abstract

Introduction

Conclusions

References

Tables

Figures



Back

Close

Full Screen / Esc

Printer-friendly Version

Interactive Discussion







## Observation error covariance matrix

The observational error covariance matrix  $\mathbf{R}$  accounts for various sources of error when comparing the hourly data selected for assimilation and their simulation which are not controlled by the inversion: measurement error, aggregation error, atmospheric model representativeness and transport error (as explained previously, uncertainties in the anthropogenic emissions and in the boundary conditions are assumed to be negligible). The first two terms are negligible compared to the model representativeness and transport error due to the high measurement standard and to solving for the fluxes at 6 h and 0.5° resolution during the inversion, respectively.

Broquet et al. (2011) derived a quantitative estimation of the model error (depending on the station height) including transport and representativeness errors based on comparisons between simulations and measurements of CO<sub>2</sub> and <sup>222</sup>Rn. Broquet et al. (2013) resumed it to provide season-dependent estimates which are used here. The model error is much higher during the winter than that during the summer. It is given for each site in Table A1 for the two months (July, December) considered in this study. We assume that the errors for two different sites are independent and that they do not bear temporal autocorrelations. Thus, the observation error covariance matrix  $\mathbf{R}$  is set diagonal. The resulting budget of observation errors at daily to monthly resolution seems reliable (Broquet et al., 2011, 2013) and, therefore, this assumption does not seem to need to be balanced by an artificial increase of the observation errors for hourly averages.

## Minimization and number of members in the Monte Carlo ensembles

We use 12 iterations of minimization for each variational inversion of the Monte Carlo ensemble experiments. This number is similar to that from Broquet et al. (2011) where they considered a longer time period for the inversions but far smaller observation networks and a smaller inversion domain, which reduces the dimensions of the minimization problem. However, here, 12 iterations were still found to be sufficient for converging

### On the potential of ICOS atmospheric CO<sub>2</sub> measurement network

N. Kadygrov et al.

Title Page

Abstract

Introduction

Conclusions

References

Tables

Figures



Back

Close

Full Screen / Esc

Printer-friendly Version

Interactive Discussion







## On the potential of ICOS atmospheric CO<sub>2</sub> measurement network

N. Kadygrov et al.

Title Page

Abstract

Introduction

Conclusions

References

Tables

Figures

◀

▶

◀

▶

Back

Close

Full Screen / Esc

Printer-friendly Version

Interactive Discussion



transport model improvement on the posterior flux uncertainties by reducing the default observation error SDs in  $\mathbf{R}$  by a factor of two. This factor roughly corresponds to the improvement of the misfits between the model and actual measurement at the site TRN (see Fig. 1 for its location), that was observed when bringing CHIMERE from the current 0.5° resolution down to a 2 km resolution using the configuration presented in Bréon et al. (2014). The underlying assumption would be that  $\sim 1$  km horizontal resolution atmospheric transport models could be used for inversions at the European scale in the near future. Hereafter, we denote by  $\mathbf{R}_{\text{ref}}$  the reference configuration of  $\mathbf{R}$  and by  $\mathbf{R}_{\text{red}}$  the one corresponding to reduced SDs.

### Test of the sensitivity to the prior uncertainty

The test of the sensitivity of the inversion system to the prior uncertainty is focused on that of the sensitivity to the spatial correlation length in  $\mathbf{B}$  (Gerbig et al., 2006) (which impacts the budget of uncertainty over large regions). The possible use of better prior flux fields based on the merging of both estimates from vegetation models and from large scale inventories (such as forest and agricultural inventories) can be expected to generate smaller-scale uncertainties than when using vegetation models while it is not obvious that local uncertainties would be decreased when adding information from inventories (since inventories only measure long term integrated NEE). Therefore, we tested the impact of reducing the spatial correlation length for the prior uncertainty in NEE from 250 to 150 km, denoting hereafter the corresponding configurations for the  $\mathbf{B}$  matrix:  $\mathbf{B}_{250}$  and  $\mathbf{B}_{150}$  respectively.

## 3 Results and discussion

### 3.1 Assessment of the performance of the actual network and system

In this section, the performance of the inversion relying on the default configuration and on the ICOS23 initial state network (i.e., the reference inversion) is analyzed as a func-

tion of the spatial scale, highlighting the main patterns of the uncertainty reduction obtained at the pixel scale to the European scale.

### 3.1.1 Analysis at the model grid scale

Figure 2a and b shows the uncertainty reduction for estimates of two-week average NEE at  $0.5^\circ$  resolution in July and December, respectively. This grid-scale uncertainty reduction reaches 65% for areas in the vicinity of the ICOS sites and decreases smoothly with distance away from measurement sites. For most of the area around eastern France – western Germany, this grid – scale uncertainty reduction ranges from 35 to 50% for July and from 20 to 40% for December. This stems from the combination of the dense observation network over that region, and from the 250 km correlation scale for the prior uncertainties, which spreads the error reduction beyond the immediate vicinity of each station where near field fluxes have a large influence on the mixing ratio at this station (Bocquet, 2005). For other parts of Europe that are not well sampled by ICOS, significant uncertainty reductions are generally seen around each site but there are large areas where the inversion has no impact at the grid scale: Scandinavian countries, the eastern part of Germany, Poland, south of the Iberian Peninsula and almost all of Eastern Europe.

The spatial structure of the uncertainty reduction and the underlying spatial extrapolation from a site is a complex combination of transport influence and of the structure of the prior uncertainty. Due to varying transport conditions, SD of the prior uncertainty at the grid scale (which is larger in summer, see below the comments on Fig. 3), and observation error (which is larger in winter), the spatial distribution of uncertainty reduction is found to vary from summer to winter. Because of the variation of prior and observation uncertainties between July and December, there is generally a larger uncertainty reduction in July (especially in Western Europe). But variations in meteorology alter (limiting or enhancing) this general behavior. The lower vertical mixing (which strengthens the sensitivity of the near ground measurements to the local fluxes) partly balances the higher observation error in December and the range of local uncertainty

## On the potential of ICOS atmospheric CO<sub>2</sub> measurement network

N. Kadygrov et al.

Title Page

Abstract

Introduction

Conclusions

References

Tables

Figures



Back

Close

Full Screen / Esc

Printer-friendly Version

Interactive Discussion





during July. It is larger than 50 % for a large majority of the countries in Western Europe and Scandinavia both in July and December.

The smallest uncertainty reduction applies to southeastern European countries where it can be smaller than 10 % (e.g., for Greece in July) indicating that the presence of stations very close to or within a given country is a requisite for bringing significant improvement to the estimates of NEE in this country. In general, the differences of the inversion skill between July and December look consistent with what has been analyzed at the pixel scale. In particular the uncertainty reduction is higher in July for western countries but higher in December for eastern countries.

### 3.1.3 Analysis at the European scale

Table 1 shows that the uncertainty in two-week-mean NEE in July averaged over the full European domain ( $6.8 \times 10^6 \text{ km}^2$  of land surface) is reduced by the inversion by 50 % down to a value of  $\sim 43 \text{ TgC month}^{-1}$  (see Table 1 for details) using the default configuration. The uncertainty reduction for December is 66 %, resulting in a posterior uncertainty of  $\sim 26 \text{ TgC month}^{-1}$ . The uncertainty reduction for the whole European domain is thus higher in December than in July. More precisely, while easterly winds in December strongly favor this period in terms of uncertainty reduction in Eastern Europe, the uncertainty reduction for NEE averaged over the reduced western European domain defined in Fig. 1c does not vary significantly with the season (66 and 64 % for July and December respectively). This lack of seasonal variation of the uncertainty reduction at the scale of the western European domain (where most of the ICOS23 stations are located) seems to contrast with the grid-scale and national scales estimations in this domain which indicated that the uncertainty reduction is generally significantly higher during summer than during winter. This contrast will be analyzed and interpreted in the following Sect. 3.1.4.

The values for the posterior uncertainty aggregated over Europe obtained with our reference configuration of the inversion are consistent with posterior uncertainties at the annual scale from the Carbon Tracker-EU system (CT-EU, Peters et al., 2010;

## On the potential of ICOS atmospheric CO<sub>2</sub> measurement network

N. Kadygrov et al.

Title Page

Abstract

Introduction

Conclusions

References

Tables

Figures



Back

Close

Full Screen / Esc

Printer-friendly Version

Interactive Discussion



http://www.carbontracker.eu) who assimilated data from 15 continuous observing sites in Europe (corresponding to a network very similar to the ICOS23 geographical configuration and with a lot of sites included in ICOS23). By assuming no error temporal correlations between uncertainties from month to month but a full temporal autocorrelation of the uncertainties within one month from a two week period to the next one (which roughly reflects the 1 month temporal autocorrelation used for the prior uncertainty in this study), such estimate, when scaled down on our study domain, yields uncertainties of  $\sim 74 \text{ TgC month}^{-1}$  for monthly fluxes.

### 3.1.4 Analysis of the variations of the uncertainty as a function of the spatial aggregation of the NEE: interpretation of the results obtained at the national and European scales

In order to examine here the dependency of the NEE uncertainty reduction to increasing spatial scales of aggregation for the analyses in July and December, we chose five locations at which we define centered areas with increasing size for which uncertainties in the average NEE are derived. These stations are located using the green circles in Fig. 1c. The five locations correspond to three observing sites of ICOS23: Trainou (TRN), Ochsenkopf (OXK), Plateau Rosa (PRS); one site of ICOS50: SMEAR II-ICOS Hyytiälä (HYY); and one point in Sweden which does not correspond to any site of the ICOS networks tested here, called SW1 hereafter (Fig. 1c). We compute the uncertainty reductions of the two-week mean NEE for July and December over 5 square (in degrees) domains centered around each site of  $1.5^\circ \times 1.5^\circ$ ,  $2.5^\circ \times 2.5^\circ$ ,  $3.5^\circ \times 3.5^\circ$ ,  $4.5^\circ \times 4.5^\circ$  and  $10.5^\circ \times 10.5^\circ$  size (which corresponds to surfaces of different size in terms of  $\text{km}^2$ ). Depending on their location and on their size, the corresponding domains expand over areas of Europe that are more or less constrained by the inversion at the pixel scale. But the variations of the uncertainty reduction when increasing the size of these domains are also strongly driven by the spatial correlations in the prior and posterior uncertainty. The results are displayed in Fig. 5.

## On the potential of ICOS atmospheric CO<sub>2</sub> measurement network

N. Kadygrov et al.

Title Page

Abstract

Introduction

Conclusions

References

Tables

Figures



Back

Close

Full Screen / Esc

Printer-friendly Version

Interactive Discussion



## On the potential of ICOS atmospheric CO<sub>2</sub> measurement network

N. Kadygrov et al.

Title Page

Abstract

Introduction

Conclusions

References

Tables

Figures



Back

Close

Full Screen / Esc

Printer-friendly Version

Interactive Discussion



The five locations used for this analysis are representative of the diversity of the situation regarding the differences between grid scale uncertainty reduction in July and in December. While the uncertainty reduction is slightly larger in July than in December for TRN, much larger in July for PRS and HYY, it is slightly larger in December at OXK and much larger in December at SW1. Furthermore, the values for these grid scale uncertainty reductions range from 15 to 50 % in July and from 7 to 47 % in December at these locations (Fig. 5).

The maximum scores of uncertainty reduction occur for spatial scales of aggregation ranging from  $10^5$  to  $10^6$  km<sup>2</sup> when considering the sites located in Western Europe. These scales approximately correspond to the range of the sizes of the European countries and it is larger than the typical area of correlation of the prior uncertainty (as defined by prior correlation lengths of 250 km). Increasing the spatial resolution generally increases the uncertainty reduction since posterior uncertainties have generally smaller correlation lengths than prior uncertainties, due to the spatial attribution error when trying to link the measurement information to local fluxes despite the atmospheric mixing. This explains the increase of uncertainty reduction from the grid scale to the “national scales”. This also explains why, for a given regional density of the measurement network, larger countries bear larger uncertainty reductions (Fig. 4). However, above such national scales, the corresponding domains include parts of Eastern Europe being poorly sampled by the ICOS23 network which explains the decrease in uncertainty reduction.

The convergence of the results around TRN, PRS and OXK to nearly 65 % uncertainty reduction in both December and July for the western European domain, and of the results at all sites to 53 % in July and 66 % in December for the whole Europe, when increasing the spatial averaging area, starts between the same  $10^5$  and  $10^6$  km<sup>2</sup> (national scale) averaging areas. For smaller areas, the differences between July and December or between different spatial locations stay similar to what is seen at the  $0.5^\circ \times 0.5^\circ$  scale.







## On the potential of ICOS atmospheric CO<sub>2</sub> measurement network

N. Kadygrov et al.

Title Page

Abstract

Introduction

Conclusions

References

Tables

Figures

◀

▶

◀

▶

Back

Close

Full Screen / Esc

Printer-friendly Version

Interactive Discussion



all spatial scales. This is because it decreases the prior uncertainty at every scale while decreasing the ability of the inversion system to extrapolate in space the information from measurement sites based on the knowledge about spatial correlations of the prior uncertainties. At 0.5° resolution, the areas of high uncertainty reduction narrows around the measurement sites and the smaller overlap of the areas of influence of these sites limits the highest local values of uncertainty reduction to 40–50 % while typical values in Western Europe now range from 20 to 40 % instead of 30 to 65 % when using  $\mathbf{B}_{250}$  (see Sect. 2.2.2 for the definition of the  $\mathbf{B}$  matrices). The uncertainty reduction for countries such as the UK, Germany and Spain decreases when the e-folding correlation length is lowered from 250 to 150 km, from more than 75–80 % to less than 70 %. For the full European domain, it decreases from 64 to 47 %.

Even though these decreases can be very large, it is critical to keep in mind that they refer to uncertainty reductions compared to a prior uncertainty which is decreased by the new configuration of  $\mathbf{B}$  (as illustrated at the country scale in Fig. A1). The posterior uncertainty in the European and two-week mean NEE in July using ICOS66 is decreased from  $\sim 33$  to  $29 \text{ TgC month}^{-1}$  when changing the configuration of  $\mathbf{B}$  from  $\mathbf{B}_{250}$  to  $\mathbf{B}_{150}$  (Table 1). Similarly, the posterior uncertainty is generally smaller at the national scale when changing the configuration of  $\mathbf{B}$  from  $\mathbf{B}_{250}$  to  $\mathbf{B}_{150}$  (Fig. A2). We thus have an expected situation for which improving the knowledge on the prior NEE improves that of the posterior NEE even if in our case, the improvement of the knowledge on the prior NEE which is tested here also decreases the ability to extrapolate in space the information from the atmospheric measurements. However, of note is that when changing the configuration of  $\mathbf{B}$  from  $\mathbf{B}_{250}$  to  $\mathbf{B}_{150}$ , we do not improve the knowledge on the prior NEE at the model grid 0.5° resolution (since modifying the correlations but not the SDs in  $\mathbf{B}$ ). Given the lower uncertainty reduction when using  $\mathbf{B}_{150}$ , the posterior uncertainties are higher at 0.5° resolution when changing the configuration of  $\mathbf{B}$  from  $\mathbf{B}_{250}$  to  $\mathbf{B}_{150}$  (Fig. A3).

### 3.4 Sensitivity to the observation error

The impact of dividing the SD of the observation error by two in the inversion configuration is tested using ICOS50 in July (compare Figs. 7a and 10b, Figs. 8a and 11b and the corresponding curves in Fig. 9). The decrease of observation error increases the weight of the measurements in the inversion and the resulting uncertainty reduction. This increase is visible at all spatial scales for the aggregation of the NEE, and relatively constant as a function of these spatial scales except at the European scale for which it is quite smaller, from 64 to 67 %. This provides the highest scores of uncertainty reduction of this study at any spatial scales, the impact of division of the observation error by two being larger than that of increasing the ICOS network configuration from ICOS50 to ICOS66.

## 4 Synthesis and conclusions

We assessed the potential of CO<sub>2</sub> mole fraction measurements from three configurations of the ICOS atmospheric network to reduce uncertainties in two-week mean European NEE at various spatial scales in summer and in winter. This assessment is based on a regional variational inverse modeling system with parameters consistent with the knowledge on uncertainties in prior estimates of NEE from ecosystem models and in atmospheric transport models. The results obtained with the various experiments from this study indicate an uncertainty reduction which ranges between ~ 50 and 80 % for the full European domain, between ~ 70 and 90 % for large countries in Western Europe (such as France, Germany, Spain, UK), where the ICOS network are denser, but below 50 % in much cases for eastern countries where there are few ICOS sites even with the ICOS66 configuration. At 0.5° resolution, if excluding results when using **B**<sub>150</sub> (for which the uncertainty reduction is applied to a different prior uncertainty), uncertainty reductions range from 30 to 65 % in the dense parts of the networks (between northern Spain and eastern Germany) while it is generally below 30 % east of Germany

### On the potential of ICOS atmospheric CO<sub>2</sub> measurement network

N. Kadygrov et al.

Title Page

Abstract

Introduction

Conclusions

References

Tables

Figures



Back

Close

Full Screen / Esc

Printer-friendly Version

Interactive Discussion









and under the framework of the preparatory phase of ICOS. It was also co-funded by the industrial chaire BridGES (supported by the Université de Versailles Saint-Quentin-en-Yvelines, the Commissariat à l'Energie Atomique et aux Energies Renouvelables, the Centre National de la Recherche Scientifique, Thales Alenia Space and Veolia). We also would like to thank the partners of the ICOS infrastructure for providing list of potential locations for future ICOS atmospheric sites.

## References

- Bocquet, M.: Grid resolution dependence in the reconstruction of an atmospheric tracer source, *Nonlin. Processes Geophys.*, 12, 219–233, doi:10.5194/npg-12-219-2005, 2005.
- Bréon, F. M., Broquet, G., Puygrenier, V., Chevallier, F., Xueref-Remy, I., Ramonet, M., Dieudonné, E., Lopez, M., Schmidt, M., Perrussel, O., and Ciais, P.: An attempt at estimating Paris area CO<sub>2</sub> emissions from atmospheric concentration measurements, *Atmos. Chem. Phys.*, 15, 1707–1724, doi:10.5194/acp-15-1707-2015, 2015.
- Broquet, G., Chevallier, F., Rayner, P. J., Aulagnier, C., Pison, I., Ramonet, M., Schmidt, M., Vermeulen, A. T., and Ciais, P.: A European summertime CO<sub>2</sub> biogenic flux inversion at mesoscale from continuous in situ mixing ratio measurements, *J. Geophys. Res.*, 116, D23303, doi:10.1029/2011JD016202, 2011.
- Broquet, G., Chevallier, F., Bréon, F.-M., Kadygrov, N., Alemanno, M., Apadula, F., Hammer, S., Haszpra, L., Meinhardt, F., Morguí, J. A., Necki, J., Piacentino, S., Ramonet, M., Schmidt, M., Thompson, R. L., Vermeulen, A. T., Yver, C., and Ciais, P.: Regional inversion of CO<sub>2</sub> ecosystem fluxes from atmospheric measurements: reliability of the uncertainty estimates, *Atmos. Chem. Phys.*, 13, 9039–9056, doi:10.5194/acp-13-9039-2013, 2013.
- Chevallier, F., Bréon, F. M., and Rayner, P. J.: Contribution of the Orbiting Carbon Observatory to the estimation of CO<sub>2</sub> sources and sinks: theoretical study in a variational data assimilation framework, *J. Geophys. Res.*, 112, D09307, doi:10.1029/2006JD007375, 2007.
- Chevallier, F., Wang, T., Ciais, P., Maignan, F., Bocquet, M., Arain, A., Cescatti, A., Chen, J., Dolman, A. J., Law, B. E., Margolis, H., Montagnani, L., and Moors, E.: What eddy-covariance measurements tell us about prior land flux errors in CO<sub>2</sub>-flux inversion schemes, *Global Biogeochem. Cy.*, 26, GB1021, doi:10.1029/2010GB003974, 2012.

## On the potential of ICOS atmospheric CO<sub>2</sub> measurement network

N. Kadygrov et al.

Title Page

Abstract

Introduction

Conclusions

References

Tables

Figures



Back

Close

Full Screen / Esc

Printer-friendly Version

Interactive Discussion



## On the potential of ICOS atmospheric CO<sub>2</sub> measurement network

N. Kadygrov et al.

Title Page

Abstract

Introduction

Conclusions

References

Tables

Figures



Back

Close

Full Screen / Esc

Printer-friendly Version

Interactive Discussion



- Claeyman, M., Attié, J.-L., Peuch, V.-H., El Amraoui, L., Lahoz, W. A., Josse, B., Joly, M., Barré, J., Ricaud, P., Massart, S., Piacentini, A., von Clarmann, T., Höpfner, M., Orphal, J., Flaud, J.-M., and Edwards, D. P.: A thermal infrared instrument onboard a geostationary platform for CO and O<sub>3</sub> measurements in the lowermost troposphere: Observing System Simulation Experiments (OSSE), *Atmos. Meas. Tech.*, 4, 1637–1661, doi:10.5194/amt-4-1637-2011, 2011.
- Edwards, D. P., Arellano Jr., A. F., and Deeter, M. N.: A satellite observation system simulation experiment for carbon monoxide in the lowermost troposphere, *J. Geophys. Res.*, 114, D14304, doi:10.1029/2008JD011375, 2009.
- Enting, I. G.: *Inverse Problems in Atmospheric Constituent Transport*, Cambridge University Press, Cambridge, UK, 2002.
- Errico, R. M., Yang, R., Privé, N. C., Tai, K.-S., Todling, R., Sienkiewicz, M. E., and Guo, J.: Development and validation of observing-system simulation experiments at NASA's Global Modeling and Assimilation Office, *Q. J. Roy. Meteor. Soc.*, 139, 1162–1178, doi:10.1002/qj.2027, 2013.
- Francey, R. J. (Ed.): Report of the Ninth WMO meeting of experts on carbon dioxide concentration and related tracer measurement techniques: Aspendale, Vic., Australia, 1–4 September 1997, World Meteorological Organization (WMO), Geneva, Series: Global Atmosphere Watch (GAW); no. 132; WMO; TD no. 952, 132 pp., 1998.
- Gerbig, C., Lin, J. C., Munger, J. W., and Wofsy, S. C.: What can tracer observations in the continental boundary layer tell us about surface-atmosphere fluxes?, *Atmos. Chem. Phys.*, 6, 539–554, doi:10.5194/acp-6-539-2006, 2006.
- Gilbert, J. C. and Lemaréchal, C.: Some numerical experiments with variable-storage quasi-Newton algorithms, *Math. Program.*, 45, 407–435, 1989.
- Gurney, K. R., Law, R. M., Denning, A. S., Rayner, P. J., Baker, D., Bousquet, P., Bruhwiler, L., Chen, Y.-H., Ciais, P., Fan, S., Fung, I. Y., Gloor, M., Heimann, M., Higuchi, K., John, J., Maki, T., Maksyutov, S., Masarie, K., Peylin, P., Prather, M., Pak, B. C., Randerson, J., Sarmiento, J., Taguchi, S., Takahashi, T., and Yuen, C.-W.: Towards robust regional estimates of CO<sub>2</sub> sources and sinks using atmospheric transport models, *Nature*, 415, 626–630, 2002.
- Halliwell Jr., G. R., Srinivasan, A., Kourafalou, V., Yang, H., Willey, D., Le Hénaff, M., and Atlas, R.: Rigorous evaluation of a fraternal twin ocean OSSE system for the Open Gulf of Mexico, *J. Atmos. Ocean. Tech.*, 31, 105–130, doi:10.1175/JTECH-D-13-00011.1, 2014.

## On the potential of ICOS atmospheric CO<sub>2</sub> measurement network

N. Kadygrov et al.

Title Page

Abstract

Introduction

Conclusions

References

Tables

Figures



Back

Close

Full Screen / Esc

Printer-friendly Version

Interactive Discussion



Hourdin, F., Musat, I., Bony, S., Braconnot, P., Codron, F., Dufresne, J. L., Fairhead, L., Filiberti, M. A., Friedlingstein, P., Grandpeix, J. Y., Krinner, G., LeVan, P., Li, Z. X., and Lott, F.: The LMDZ4 general circulation model: climate performance and sensitivity to parametrized physics with emphasis on tropical convection, *Clim. Dynam.*, 27, 787–813, doi:10.1007/s00382-006-0158-0, 2006.

Houweling, S., Breon, F.-M., Aben, I., Rödenbeck, C., Gloor, M., Heimann, M., and Ciais, P.: Inverse modeling of CO<sub>2</sub> sources and sinks using satellite data: a synthetic inter-comparison of measurement techniques and their performance as a function of space and time, *Atmos. Chem. Phys.*, 4, 523–538, doi:10.5194/acp-4-523-2004, 2004.

Hungershofer, K., Breon, F.-M., Peylin, P., Chevallier, F., Rayner, P., Klonecki, A., Houweling, S., and Marshall, J.: Evaluation of various observing systems for the global monitoring of CO<sub>2</sub> surface fluxes, *Atmos. Chem. Phys.*, 10, 10503–10520, doi:10.5194/acp-10-10503-2010, 2010.

Kadygrov, N., Maksyutov, S., Eguchi, N., Aoki, T., Nakazawa, T., Yokota, T., and Inoue, G.: Role of simulated GOSAT total column CO<sub>2</sub> observations in surface CO<sub>2</sub> flux uncertainty reduction, *J. Geophys. Res.*, 114, D21208, doi:10.1029/2008JD011597, 2009.

Krinner, G., Viovy, N., de Noblet-Ducoudré, N., Ogée, J., Polcher, J., Friedlingstein, P., Ciais, P., Sitch, S., and Prentice, I. C.: A dynamic global vegetation model for studies of the coupled atmosphere-biosphere system, *Global Biogeochem. Cy.*, 19, GB1015, doi:10.1029/2003GB002199, 2005.

Lauvaux, T., Uliasz, M., Sarrat, C., Chevallier, F., Bousquet, P., Lac, C., Davis, K. J., Ciais, P., Denning, A. S., and Rayner, P. J.: Mesoscale inversion: first results from the CERES campaign with synthetic data, *Atmos. Chem. Phys.*, 8, 3459–3471, doi:10.5194/acp-8-3459-2008, 2008.

Lauvaux, T., Schuh, A. E., Uliasz, M., Richardson, S., Miles, N., Andrews, A. E., Sweeney, C., Diaz, L. I., Martins, D., Shepson, P. B., and Davis, K. J.: Constraining the CO<sub>2</sub> budget of the corn belt: exploring uncertainties from the assumptions in a mesoscale inverse system, *Atmos. Chem. Phys.*, 12, 337–354, doi:10.5194/acp-12-337-2012, 2012.

Law, R. M., Peters, W., Roedenbeck, C., Aulagnier, C., Baker, I., Bergmann, D. J., Bousquet, P., Brandt, J., Bruhwiler, L., Cameron-Smith, P. J., Christensen, J. H., Delage, F., Denning, A. S., Fan, S., Geels, C., Houweling, S., Imasu, R., Karstens, U., Kawa, S. R., Kleist, J., Krol, M. C., Lin, S. J., Lokupitiya, R., Maki, T., Maksyutov, S., Niwa, Y., Onishi, R., Parazoo, N., Patra, P. K., Pieterse, G., Rivier, L., Satoh, M., Serrar, S., Taguchi, S., Takigawa, M., Vau-



## On the potential of ICOS atmospheric CO<sub>2</sub> measurement network

N. Kadygrov et al.

Title Page

Abstract

Introduction

Conclusions

References

Tables

Figures



Back

Close

Full Screen / Esc

Printer-friendly Version

Interactive Discussion

tard, R., Vermeulen, A. T., and Zhu, Z.: TransCom model simulations of hourly atmospheric CO<sub>2</sub>: experimental overview and diurnal cycle results for 2002, *Global Biogeochem. Cy.*, 22, GB3009, doi:10.1029/2007gb003050, 2008.

Masutani, M., Schlatter, T. W., Errico, R. M., Stoffelen, A., Andersson, E., Lahoz, W., Woollen, J. S., Emmitt, G. D., Riishøjgaard, L.-P., and Lord, S. J.: Observing system simulation experiments, in: *Data Assimilation: Making Sense of Observations*, edited by: Lahoz, W. A., Khattatov, B., and Ménard, R., Springer, Berlin, 647–679, 2010.

Meesters, A. G. C. A., Tolk, L. F., Peters, W., Hutjes, R. W. A., Veling, O. S., Elbers, J. A., Vermeulen, A. T., van der Laan, S., Neubert, R. E. M., Meijer, H. A. J., and Dolman, A. J.: Inverse carbon dioxide flux estimates for the Netherlands, *J. Geophys. Res.*, 117, D20306, doi:10.1029/2012JD017797, 2012.

Peters, W., Krol, M. C., Van Der Werf, G. R., Houweling, S., Jones, C. D., Hughes, J., Schaefer, K., Masarie, K. A., Jacobson, A. R., Miller, J. B., Cho, C. H., Ramonet, M., Schmidt, M., Ciattaglia, L., Apadula, F., Heltai, D., Meinhardt, F., Di Sarra, A. G., Piacentino, S., Sferlazzo, D., Aalto, T., Hatakka, J., Strom, J., Haszpra, L., Meijer, H. A. J., Van Der Laan, S., Neubert, R. E. M., Jordan, A., Rodo, X., Morgui, J.-A., Vermeulen, A. T., Popa, E., Rozanski, K., Zimnoch, M., Manning, A. C., Leuenberger, M., Uglietti, C., Dolman, A. J., Ciais, P., Heimann, M., and Tans, P. P.: Seven years of recent European net terrestrial carbon dioxide exchange constrained by atmospheric observations, *Glob. Change Biol.*, 16, 1317–1337, doi:10.1111/j.1365-2486.2009.02078.x, 2010.

Peylin, P., Houweling, S., Krol, M. C., Karstens, U., Rödenbeck, C., Geels, C., Vermeulen, A., Badawy, B., Aulagnier, C., Pregar, T., Delage, F., Pieterse, G., Ciais, P., and Heimann, M.: Importance of fossil fuel emission uncertainties over Europe for CO<sub>2</sub> modeling: model inter-comparison, *Atmos. Chem. Phys.*, 11, 6607–6622, doi:10.5194/acp-11-6607-2011, 2011.

Peylin, P., Law, R. M., Gurney, K. R., Chevallier, F., Jacobson, A. R., Maki, T., Niwa, Y., Patra, P. K., Peters, W., Rayner, P. J., Rödenbeck, C., van der Laan-Luijckx, I. T., and Zhang, X.: Global atmospheric carbon budget: results from an ensemble of atmospheric CO<sub>2</sub> inversions, *Biogeosciences*, 10, 6699–6720, doi:10.5194/bg-10-6699-2013, 2013.

Riishøjgaard, L. P., Ma, Z., Masutani, M., Woollen, J. S., Emmitt, G. D., Wood, S. A., and Greco, S.: Observation system simulation experiments for a global wind observing sounder, *Geophys. Res. Lett.*, 39, L17805, doi:10.1029/2012GL051814, 2012.

## On the potential of ICOS atmospheric CO<sub>2</sub> measurement network

N. Kadygrov et al.

Title Page

Abstract

Introduction

Conclusions

References

Tables

Figures

◀

▶

◀

▶

Back

Close

Full Screen / Esc

Printer-friendly Version

Interactive Discussion

- Rödenbeck, C., Houweling, S., Gloor, M., and Heimann, M.: CO<sub>2</sub> flux history 1982–2001 inferred from atmospheric data using a global inversion of atmospheric transport, *Atmos. Chem. Phys.*, 3, 1919–1964, doi:10.5194/acp-3-1919-2003, 2003.
- Schmidt, H., Derognat, C., Vautard, R., and Beekmann, M.: A comparison of simulated and observed ozone mixing ratios for the summer of 1998 in Western Europe, *Atmos. Environ.*, 35, 6277–6297, doi:10.1016/S1352-2310(01)00451-4, 2001.
- Schuh, A. E., Denning, A. S., Corbin, K. D., Baker, I. T., Uliasz, M., Parazoo, N., Andrews, A. E., and Worthy, D. E. J.: A regional high-resolution carbon flux inversion of North America for 2004, *Biogeosciences*, 7, 1625–1644, doi:10.5194/bg-7-1625-2010, 2010.
- Schulze, E. D., Ciais, P., Luysaert, S., Schrumppf, M., Janssens, I. A., Thiruchittampalam, B., Theloke, J., Saurat, M., Bringezu, S., Lelieveld, J., Lohila, A., Rebmann, C., Jung, M., Bastviken, D., Abril, G., Grassi, G., Leip, A., Freibauer, A., Kutsch, W., Don, A., Nieschulze, J., Borner, A., Gash, J. H., and Dolman, A. J.: The European carbon balance. Part 4: integration of carbon and other trace-gases fluxes, *Global Change Biol.*, 16, 1451–1469, 2010.
- Takahashi, T., Sutherland, S. C., Wanninkhof, R., Sweeney, C., Feely, R. A., Chipman, D. W., Hales, B., Friederich, G., Chavez, F., Sabine, C., Watson, A., Bakker, D. C. E., Schuster, U., Metzl, N., Yoshikawa-Inoue, H., Ishii, M., Midorikawa, T., Nojiri, Y., Körtzinger, A., Steinhoff, T., Hoppema, M., Olafsson, J., Arnarson, T. S., Tilbrook, B., Johannessen, T., Olsen, A., Bellerby, R., Wong, C. S., Delille, B., Bates, N. R., and de Baar, H. J. W.: Climatological mean and decadal change in surface ocean pCO<sub>2</sub>, and net sea–air CO<sub>2</sub> flux over the global oceans, *Deep-Sea Res. Pt. II*, 56, 554–577, doi:10.1016/j.dsr2.2008.12.009, 2009.
- Timmermans, R. M. A., Schaap, M., Elbern, H., Siddans, R., Tjemkes, S., Vautard, R., and Buitjes, P.: An observing system simulation experiment (OSSE) for aerosol optical depth from satellites, *J. Atmos. Ocean. Tech.*, 26, 2673–2682, 2009a.
- Timmermans, R. M. A., Segers, A. J., Buitjes, P. J. H., Vautard, R., Siddans, R., Elbern, H., Tjemkes, S. A. T., and Schaap, M.: The added value of a proposed satellite imager for ground level particulate matter analyses and forecasts, *IEEE J. Sel. Top. Appl.*, 2, 271–283, 2009b.
- Tolk, L. F., Dolman, A. J., Meesters, A. G. C. A., and Peters, W.: A comparison of different inverse carbon flux estimation approaches for application on a regional domain, *Atmos. Chem. Phys.*, 11, 10349–10365, doi:10.5194/acp-11-10349-2011, 2011.
- Weaver, A. T., Vialard, J., Anderson, D. L. T., and Delecluse, P.: Three- and four-dimensional variational assimilation with an ocean general circulation model of the tropical Pacific Ocean.

Part I: formulation, internal diagnostics and consistency checks, Mon. Weather Rev., 131, 1360–1378, 2003.

World Meteorological Organization: “Scientific Requirements” in Report of the WMO/UNEP/ICSU Meeting on Instruments, Standardization and measurement techniques for atmospheric CO<sub>2</sub>, Geneva, Switzerland, 8–11 September 1981.

5 Ziehn, T., Nickless, A., Rayner, P. J., Law, R. M., Roff, G., and Fraser, P.: Greenhouse gas network design using backward Lagrangian particle dispersion modelling – Part 1: Methodology and Australian test case, Atmos. Chem. Phys., 14, 9363–9378, doi:10.5194/acp-14-9363-2014, 2014.

## ACPD

15, 14221–14273, 2015

### On the potential of ICOS atmospheric CO<sub>2</sub> measurement network

N. Kadygrov et al.

Title Page

Abstract

Introduction

Conclusions

References

Tables

Figures



Back

Close

Full Screen / Esc

Printer-friendly Version

Interactive Discussion



## On the potential of ICOS atmospheric CO<sub>2</sub> measurement network

N. Kadygrov et al.

**Table 1.** Uncertainty reduction in two-week and European mean NEE for July and December as a function of the observation network and of the configuration of the inversion parameters ( $\mathbf{B}_{250}$  or  $\mathbf{B}_{150}$  for  $\mathbf{B}$  and  $\mathbf{R}_{\text{ref}}$  or  $\mathbf{R}_{\text{red}}$  for  $\mathbf{R}$ ).

	Month	$\mathbf{B}$	$\mathbf{R}$	Prior uncertainty (TgC month <sup>-1</sup> )	Posterior uncertainty (TgC month <sup>-1</sup> )	NEE from ORCHIDEE (TgC month <sup>-1</sup> )	Uncertainty reduction (%)
ICOS23	Jul	$\mathbf{B}_{250}$	$\mathbf{R}_{\text{ref}}$	91.2	42.6	-201.6	53
	Dec	$\mathbf{B}_{250}$	$\mathbf{R}_{\text{ref}}$	74.9	25.5	80.3	66
ICOS50	Jul	$\mathbf{B}_{250}$	$\mathbf{R}_{\text{ref}}$	91.2	32.4	-201.6	64
	Dec	$\mathbf{B}_{250}$	$\mathbf{R}_{\text{ref}}$	74.9	19.5	80.3	74
	Jul	$\mathbf{B}_{250}$	$\mathbf{R}_{\text{red}}$	91.2	30.4	-201.6	67
ICOS66	Jul	$\mathbf{B}_{250}$	$\mathbf{R}_{\text{ref}}$	91.2	32.8	-201.6	64
	Dec	$\mathbf{B}_{250}$	$\mathbf{R}_{\text{ref}}$	74.9	15.4	80.3	79
	Jul	$\mathbf{B}_{150}$	$\mathbf{R}_{\text{ref}}$	55.0	29.2	-201.6	47



## On the potential of ICOS atmospheric CO<sub>2</sub> measurement network

N. Kadygrov et al.

Table A1. Continued.

Network	Site	Country	Code	Type	Lon	Lat	Height m a.g.l.	Elevation m a.s.l.	Assim. Window	Obs. Err. (ppm) Jul	Dec	
ICOS50	Kresin u Pacova	CZ	kre	TT	15.08	49.57	250	790	12–20	4.2–7.2	10.2–15.2	
	Hohenpeißenberg	DE	hpb	TT	11.01	47.8	159	1106	00–06	3.6	3.6	
	Zugspitze	DE	zug	G	10.98	47.42	10	2660	00–06	3.6	3.6	
	Riso Meteorological Mast	DK	ris	TT	12.09	55.65	125	130	12–20	4.2–7.2	10.2–15.2	
	Hovsøre Wind Test Station	DK	hov	TT	8.15	56.44	116	116	12–20	4.2–7.2	10.2–15.2	
	Carnsore Point EMEP monitoring Station	IR	crn	G	–6.33	52.06	3	3	12–20	4.2–7.2	10.2–15.2	
	Malin Head Synoptic Meteorological Station	IR	mlđ	G	–7.37	55.38	3	13	12–20	4.2–7.2	10.2–15.2	
	Katowice Kosztowy	PL	kat	TT	19.12	50.19	355	655	12–20	4.2–7.2	10.2–15.2	
	Piła Rusionow	PL	pil	TT	16.26	53.17	320	455	12–20	4.2–7.2	10.2–15.2	
	Jemiolow	PL	jem	TT	15.28	52.35	314	475	12–20	4.2–7.2	10.2–15.2	
	Hyltemossa	SE	hyl	TT	13.42	56.1	150	255	12–20	4.2–7.2	10.2–15.2	
	Observatoire Pérenne de l'Environnement	FR	ope	TT	5.36	48.48	120	512	12–20	4.2–7.2	10.2–15.2	
	Observatoire de Haute Provence	FR	ohp	TT	5.71	43.93	100	740	12–20	4.2–7.2	10.2–15.2	
	Pic du Midi	FR	pdm	G	0.14	42.94	10	2887	00–06	3.6	3.6	
	SMEAR II Hyytiälä	FI	hyy	TT	24.29	61.85	127	308	12–20	4.2–7.2	10.2–15.2	
	Puijo-Koli ICOS eastern Finland	FI	pui	TT	27.65	62.9	176	406	12–20	4.2–7.2	10.2–15.2	
	Utö - Baltic sea	FI	uto	G	21.38	59.78	60	68	12–20	4.2–7.2	10.2–15.2	
	Finokallia	GR	fik	G	25.67	35.34	2	152	12–20	4.2–7.2	10.2–15.2	
	Birkenes Observatory	NO	bir	G	8.25	58.38	gl	190	12–20	4.2–7.2	10.2–15.2	
	Andøya Observatory	NO	and	G	16.01	69.27	gl	380	12–20	4.2–7.2	10.2–15.2	
	Svartberget	SE	sva	TT	19.78	64.26	150	385	12–20	4.2–7.2	10.2–15.2	
	Tacolneston (norfolk)	UK	tac	G	1.14	52.52	191	261	12–20	4.2–7.2	10.2–15.2	
	Ridge Hill	UK	rhi	G	–2.54	52	152	356	12–20	4.2–7.2	10.2–15.2	
	Delta Ebre	ES	dec	TT	0.79	40.74	11	16	12–20	4.2–7.2	10.2–15.2	
	Valderejo	ES	val	TT	–3.21	42.87	25	1100	00–06	3.6	3.6	
	Xures-Invernadero	ES	xic	TT	–8.02	41.98	30	902	12–20	4.2–7.2	10.2–15.2	
	Ispira	IT	isp	G	8.63	45.81	40	230	12–20	4.2–7.2	10.2–15.2	
	ICOS66	Lindenberg	DE	lin	TT	14.12	52.21	99	192	12–20	4.2–7.2	10.2–15.2
		Mannheim	DE	man	TT	8.49	49.49	213	323	12–20	4.2–7.2	10.2–15.2
		Gartow 2	DE	grt	TT	11.44	53.07	344	410	12–20	4.2–7.2	10.2–15.2
Messkirch/Rohrdorf		DE	msr	TT	9.12	48.02	240	892	12–20	4.2–7.2	10.2–15.2	
Wesell		DE	wsl	TT	6.57	51.65	321	340	12–20	4.2–7.2	10.2–15.2	
Helgoland		DE	hlđ	G	7.9	54.18	10	40	12–20	4.2–7.2	10.2–15.2	
Iznajar		ES	izn	TT	–4.38	37.28	5	555	12–20	4.2–7.2	10.2–15.2	
Hengelo		NL	hen	G	6.75	52.34	70	80	12–20	4.2–7.2	10.2–15.2	
Goes		NL	goe	G	3.78	51.48	70	70	12–20	4.2–7.2	10.2–15.2	
Peel		NL	pee	G	5.98	51.37	70	80	12–20	4.2–7.2	10.2–15.2	
Noordzee		NL	nse	G	4.73	54.85	50	50	12–20	4.2–7.2	10.2–15.2	
Cap Corse		FR	cor	G	9.35	42.93	35	85	12–20	4.2–7.2	10.2–15.2	
Roc Tredudon		FR	roc	G	–3.91	48.41	10	373	12–20	4.2–7.2	10.2–15.2	
Alfabia		ES	alf	TT	2.72	39.74	gl	1069	00–06	3.6	3.6	
Saissac		FR	sai	TT	–2.1	43.39	300	800	00–06	3.6	3.6	
NIO		FR	nio	TT	0.05	46.19	330	503	12–20	4.2–7.2	10.2–15.2	

Title Page

Abstract

Introduction

Conclusions

References

Tables

Figures

◀

▶

◀

▶

Back

Close

Full Screen / Esc

Printer-friendly Version

Interactive Discussion



**Table A2.** NEE uncertainty budget for European countries for July 2007 estimated using the reference inversion configuration and different atmospheric CO<sub>2</sub> networks. Uncertainty reduction values (UR) are shown in the last two columns.

Country	NEE,	NEE prior unc.	NEE post. Unc.		UR (%)	
	Tg C country <sup>-1</sup> month <sup>-1</sup>	Tg C country <sup>-1</sup> month <sup>-1</sup>	Tg C country <sup>-1</sup> month <sup>-1</sup>	Tg C country <sup>-1</sup> month <sup>-1</sup>	ICOS23	ICOS66
Austria	-3.95	4.60	1.49	1.56	68	66
Belgium	-1.05	1.88	0.69	0.69	63	63
Bulgaria	-1.22	5.72	5.43	4.06	5	29
Croatia	-1.64	2.27	1.17	1.13	48	50
Cyprus	0.04	0.18	0.18	0.18	0	1
Czech Republic	-4.35	4.08	2.06	1.52	50	63
Denmark	-1.97	1.74	1.35	0.76	22	57
Estonia	-2.67	2.37	1.66	1.42	30	40
Finland	-8.37	11.56	5.92	3.14	49	73
France	-17.16	18.41	3.52	3.04	81	84
Germany	-16.00	14.20	4.73	2.73	67	81
Greece	0.09	3.58	3.45	2.89	4	19
Hungary	-2.19	4.95	2.61	2.31	47	53
Ireland	-2.49	2.42	1.68	1.27	30	48
Italy	-4.44	9.83	4.24	3.82	57	61
Latvia	-3.61	3.32	2.33	2.22	30	33
Lithuania	-3.92	3.42	2.02	2.10	41	39
Luxembourg	-0.12	0.17	0.10	0.10	42	44
Netherlands	-0.97	1.99	0.65	0.50	68	75
Norway	-6.02	9.65	4.85	4.65	50	52
Poland	-21.10	13.26	5.02	4.24	62	68
Portugal	-1.17	4.24	3.71	2.80	12	34
Romania	-7.14	10.79	9.14	8.34	15	23
Slovakia	-2.82	2.59	1.30	1.30	50	50
Slovenia	-1.17	1.04	0.48	0.43	54	58
Spain	-3.54	19.90	7.16	3.97	64	80
Sweden	-9.84	16.50	7.53	5.62	54	66
Switzerland	-1.72	2.61	1.03	0.68	60	74
UK	-8.52	7.56	2.11	1.59	72	79

**On the potential of ICOS atmospheric CO<sub>2</sub> measurement network**

N. Kadygrov et al.

Title Page

Abstract Introduction

Conclusions References

Tables Figures

◀ ▶

◀ ▶

Back Close

Full Screen / Esc

Printer-friendly Version

Interactive Discussion



## On the potential of ICOS atmospheric CO<sub>2</sub> measurement network

N. Kadygrov et al.

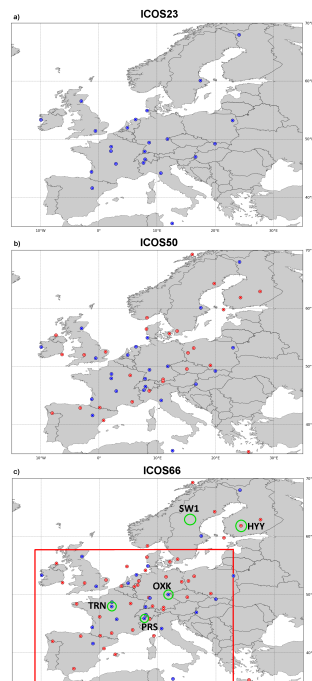


**Figure 1.** Site location for the different ICOS network configurations used in this study: **(a)** ICOS23 **(b)** ICOS50 **(c)** ICOS66. Dark blue circles correspond to ICOS23 and the red circles are the new sites for ICOS50 and ICOS66 compared to ICOS23. The European domain ( $\sim 6.8 \times 10^6 \text{ km}^2$  of land surface) covered by these figures corresponds to the domain of the configuration of the CHIMERE atmospheric transport model used in this study. The red rectangle in **(c)** corresponds to a western European domain (WE domain,  $\sim 3.5 \times 10^6 \text{ km}^2$  of land surface) which is used for some of the present analysis because it is significantly better sampled by the ICOS networks than other areas. Green circles in **(c)** are the station locations used for the study of the uncertainty reduction as a function of the spatial scale of the aggregation around each station (in Sect. 3.1.4).

Title Page

Abstract

Introduction

Conclusions

References

Tables

Figures

◀

▶

◀

▶

Back

Close

Full Screen / Esc

Printer-friendly Version

Interactive Discussion



## On the potential of ICOS23 atmospheric CO<sub>2</sub> measurement network

N. Kadygrov et al.

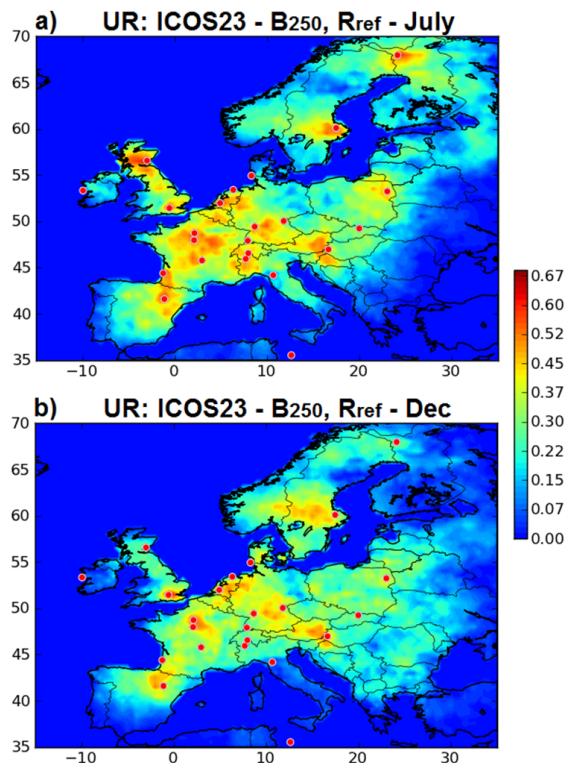


**Figure 2.** Uncertainty reduction (theoretically comprised between 0 and 1) for two-week mean NEE at 0.5° resolution in July (a) and in December (b) when using ICOS23 (red dots) and the reference inversion setup. Red/blue colors indicate relatively high/low uncertainty reduction (with min = 0, max = 0.68 in the color scale).

[Title Page](#)[Abstract](#)[Introduction](#)[Conclusions](#)[References](#)[Tables](#)[Figures](#)[◀](#)[▶](#)[◀](#)[▶](#)[Back](#)[Close](#)[Full Screen / Esc](#)[Printer-friendly Version](#)[Interactive Discussion](#)

## On the potential of ICOS atmospheric CO<sub>2</sub> measurement network

N. Kadygrov et al.

Title Page

Abstract

Introduction

Conclusions

References

Tables

Figures

◀

▶

◀

▶

Back

Close

Full Screen / Esc

Printer-friendly Version

Interactive Discussion

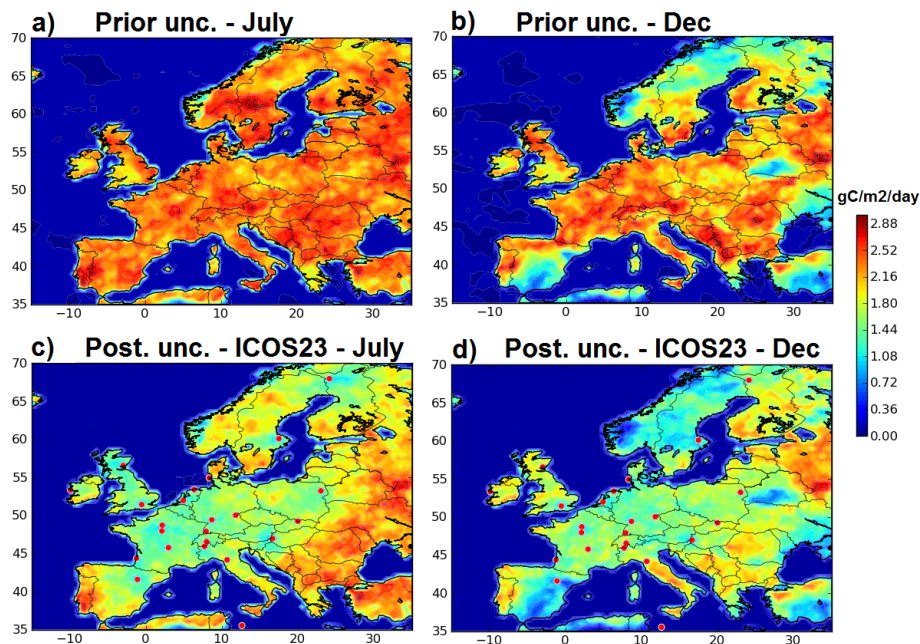


**Figure 3.** SDs ( $\text{g C m}^{-2} \text{ day}^{-1}$ ) of the prior (**a, b**) and posterior (**c, d**) uncertainties in two-week mean NEE at  $0.5^\circ$  resolution for (**a, c**) July and (**b, d**) December. Posterior uncertainties are given for inversions using ICOS23 (red dots) and the reference inversion setup. Red/blue colors indicate relatively high/low uncertainties (with  $\text{min} = 0 \text{ g C m}^{-2} \text{ day}^{-1}$ ,  $\text{max} = 3 \text{ g C m}^{-2} \text{ day}^{-1}$  in the color scale).

## On the potential of ICOS23 atmospheric CO<sub>2</sub> measurement network

N. Kadygrov et al.

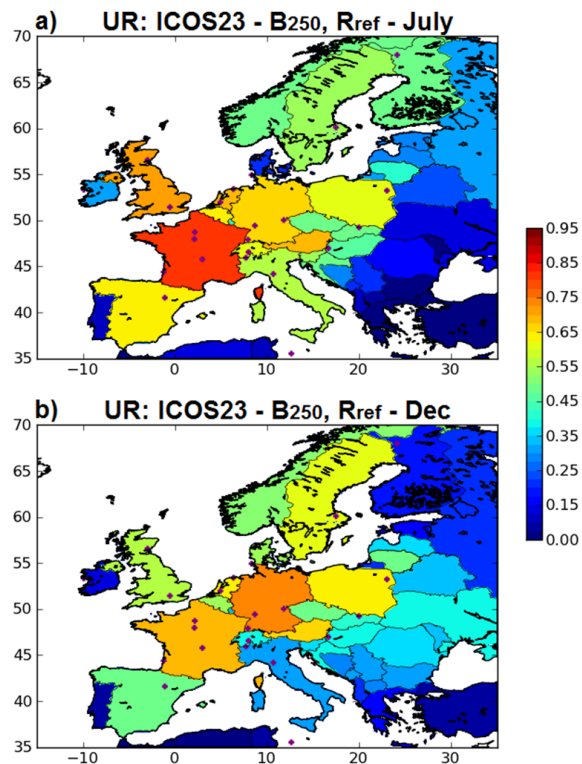


**Figure 4.** Uncertainty reduction (theoretically comprised between 0 and 1) for two-week mean NEE at the country scale for July **(a)** and December **(b)** when using ICOS23 and the reference inversion configuration. Red/blue colors indicate relatively high/low uncertainty reduction (with min = 0, max = 0.95 in the color scale).

[Title Page](#)[Abstract](#)[Introduction](#)[Conclusions](#)[References](#)[Tables](#)[Figures](#)[◀](#)[▶](#)[◀](#)[▶](#)[Back](#)[Close](#)[Full Screen / Esc](#)[Printer-friendly Version](#)[Interactive Discussion](#)

**On the potential of ICOS atmospheric CO<sub>2</sub> measurement network**

N. Kadygrov et al.

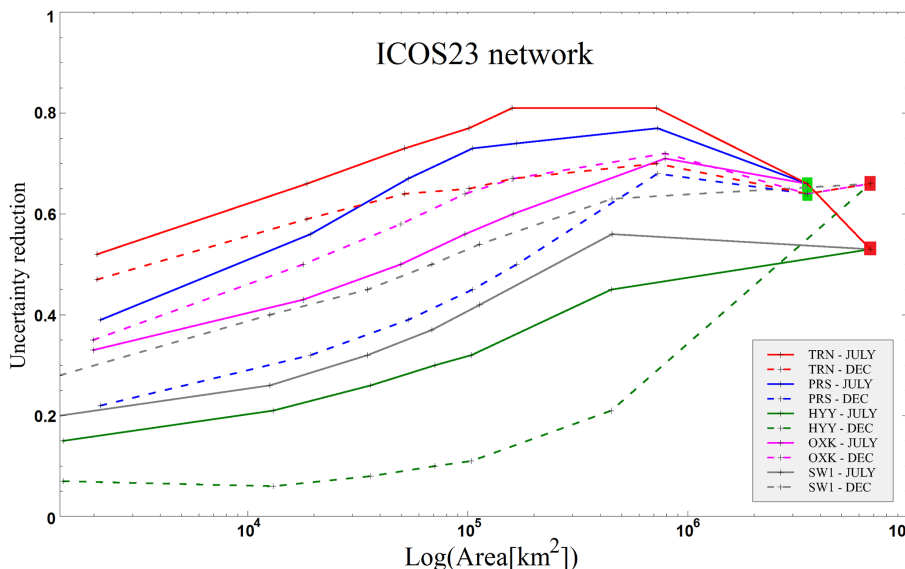


**Figure 5.** Uncertainty reduction (theoretically comprised between 0 and 1) for two-week mean NEE in July and December 2007 using ICOS23 and the reference configuration of the inversion, as a function of the size (logarithmic scale) of the spatial averaging area around each station TRN (red curves), PRS (blue curves), HYY (green curves), OXK (pink curves) and SW1 (grey curves; see the locations in Fig. 1c). Solid and dash lines correspond to results for July and December respectively (see the legend within the figure). The results of uncertainty reduction for the whole European domain are included (red rectangle). The results for the western European domain defined in Fig. 1c are included on curves corresponding to sites which are located in this domain (TRN, PRS and OXK, see the green rectangle).

Title Page

Abstract Introduction

Conclusions References

Tables Figures

◀ ▶

◀ ▶

Back Close

Full Screen / Esc

Printer-friendly Version

Interactive Discussion



## On the potential of ICOS atmospheric CO<sub>2</sub> measurement network

N. Kadygrov et al.

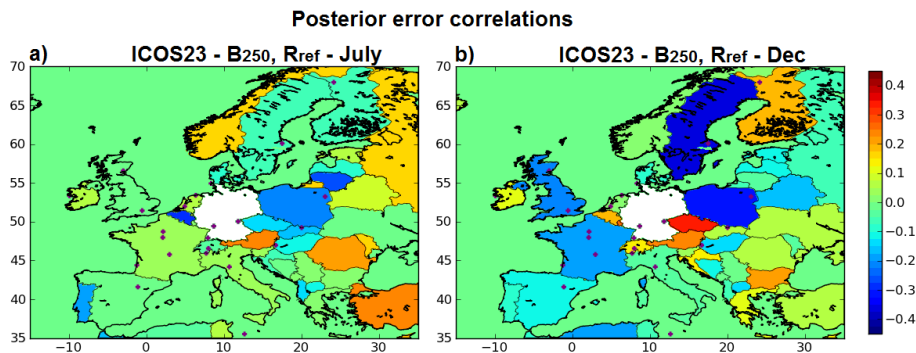


**Figure 6.** Correlations of the posterior uncertainties in two-week mean NEE between Germany and the other European countries in July (a) and December (b) from the reference inversions with ICOS23. Germany is masked in white. Red/blue colors indicate relatively high positive/negative correlations (with min = -0.45, max = 0.45 in the color scale).

Title Page

Abstract

Introduction

Conclusions

References

Tables

Figures

◀

▶

◀

▶

Back

Close

Full Screen / Esc

Printer-friendly Version

Interactive Discussion



## On the potential of ICOS atmospheric CO<sub>2</sub> measurement network

N. Kadygrov et al.

Title Page

Abstract

Introduction

Conclusions

References

Tables

Figures

◀

▶

◀

▶

Back

Close

Full Screen / Esc

Printer-friendly Version

Interactive Discussion

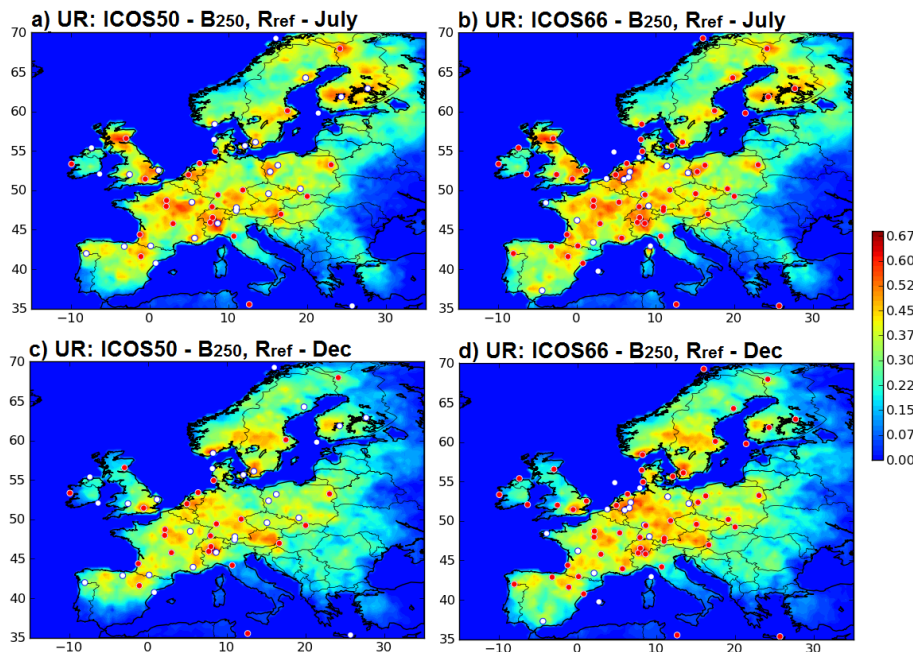


**Figure 7.** Uncertainty reduction (theoretically comprised between 0 and 1) for two-week mean NEE at 0.5° resolution in July (**a, b**) and December (**c, d**) when using ICOS50 (**a, c**) and ICOS66 (**b, d**) and the reference inversion configuration. Red dots corresponds to the ICOS23 (**a, c**) or ICOS50 (**b, d**) sites while white dots correspond to the additional sites included in ICOS50 or ICOS66 respectively. Red/blue colors indicate relatively high/low uncertainty reduction (with min = 0, max = 0.68 in the color scale).

## On the potential of ICOS atmospheric CO<sub>2</sub> measurement network

N. Kadygrov et al.

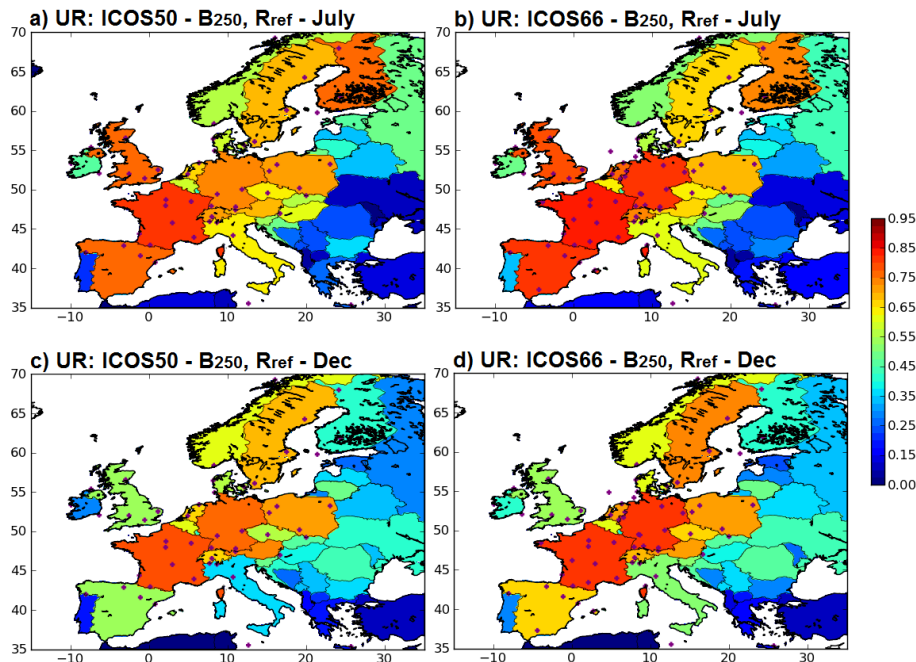


**Figure 8.** Uncertainty reduction (theoretically comprised between 0 and 1) for two-week mean NEE at the country scale in July (**a, b**) and December (**c, d**), when using ICOS50 (**a, c**) and ICOS66 (**b, d**). Red/blue colors indicate relatively high/low uncertainty reduction (with min = 0, max = 0.95 in the color scale).

[Title Page](#)[Abstract](#)[Introduction](#)[Conclusions](#)[References](#)[Tables](#)[Figures](#)[◀](#)[▶](#)[◀](#)[▶](#)[Back](#)[Close](#)[Full Screen / Esc](#)[Printer-friendly Version](#)[Interactive Discussion](#)

## On the potential of ICOS atmospheric CO<sub>2</sub> measurement network

N. Kadygrov et al.

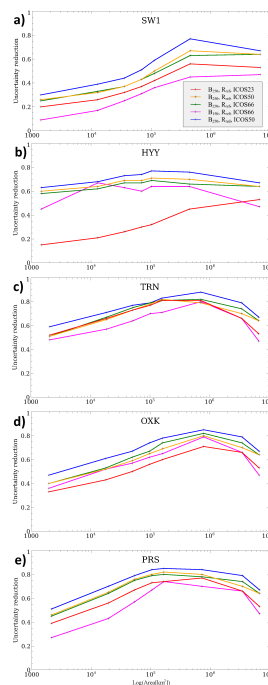


**Figure 9.** Uncertainty reduction (theoretically comprised between 0 and 1) for two-week mean NEE for July 2007 as a function of the size (in logarithmic scale) of the spatial averaging area centered on **(a)** SW1, **(b)** HYY, **(c)** TRN, **(d)** OXK, and **(e)** PRS. Red, orange, green lines: results with the reference configuration of the inversion using ICOS23, ICOS50 and ICOS66 respectively; blue: results when using ICOS50 and the inversion configuration with  $\mathbf{R} = \mathbf{R}_{\text{red}}$ ; pink: results when using ICOS66 and the inversion configuration with  $\mathbf{B} = \mathbf{B}_{150}$ . The results of uncertainty reduction for the whole European domain are included systematically. The results for the western European domain defined in Fig. 1c are included on curves corresponding to sites which are located in this domain (TRN, PRS and OXK).

[Title Page](#)
[Abstract](#)
[Introduction](#)
[Conclusions](#)
[References](#)
[Tables](#)
[Figures](#)
[Back](#)
[Close](#)
[Full Screen / Esc](#)
[Printer-friendly Version](#)
[Interactive Discussion](#)




## On the potential of ICOS atmospheric CO<sub>2</sub> measurement network

N. Kadygrov et al.

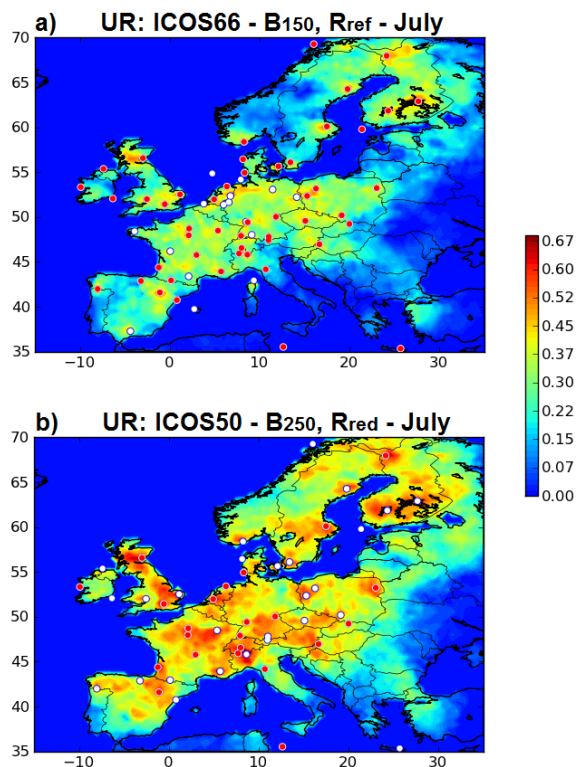


**Figure 10.** Uncertainty reduction (theoretically comprised between 0 and 1) for two-week mean NEE at 0.5° horizontal resolution in July when modifying the inversion configuration from the reference one: using  $B_{150}$  instead of  $B_{250}$  and ICOS66 **(a)** using  $R_{red}$  instead of  $R_{ref}$  and ICOS50 **(b)**. Red dots corresponds to the ICOS23 **(b)** or ICOS50 **(a)** sites while white dots correspond to the additional sites included in ICOS50 or ICOS66 respectively. Red/blue colors indicate relatively high/low uncertainty reduction (with min = 0, max = 0.68 in the color scale).

[Title Page](#)
[Abstract](#)
[Introduction](#)
[Conclusions](#)
[References](#)
[Tables](#)
[Figures](#)
[Back](#)
[Close](#)
[Full Screen / Esc](#)
[Printer-friendly Version](#)
[Interactive Discussion](#)

## On the potential of ICOS atmospheric CO<sub>2</sub> measurement network

N. Kadygrov et al.

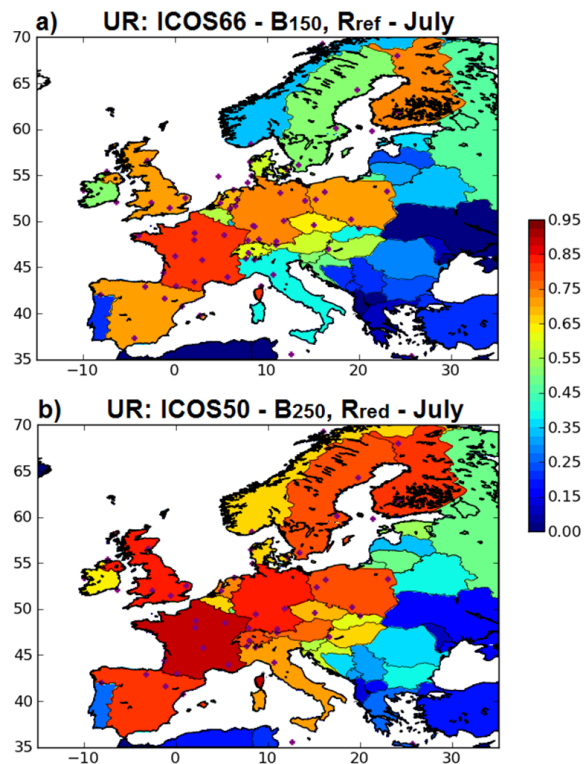


**Figure 11.** Uncertainty reduction (theoretically comprised between 0 and 1) for two-week mean NEE at the country scale in July when modifying the inversion configuration from the reference one by using  $B_{150}$  instead of  $B_{250}$  and ICOS66 (a) using  $R_{red}$  instead of  $R_{ref}$  and ICOS50 (b). Red/blue colors indicate relatively high/low uncertainty reduction (with min = 0, max = 0.95 in the color scale).

[Title Page](#)[Abstract](#)[Introduction](#)[Conclusions](#)[References](#)[Tables](#)[Figures](#)[◀](#)[▶](#)[◀](#)[▶](#)[Back](#)[Close](#)[Full Screen / Esc](#)[Printer-friendly Version](#)[Interactive Discussion](#)

On the potential of  
ICOS atmospheric  
CO<sub>2</sub> measurement  
network

N. Kadygrov et al.

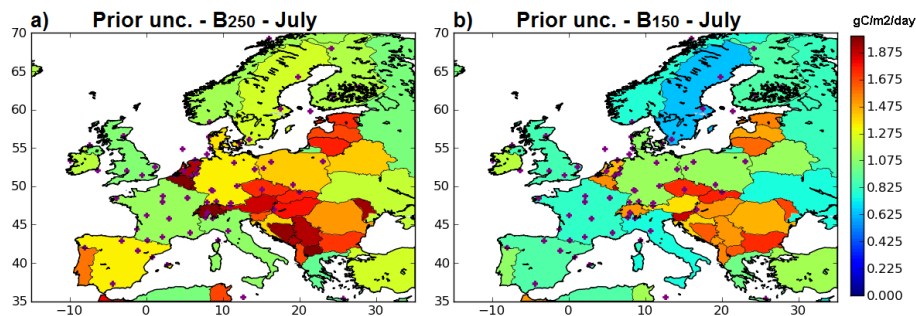


**Figure A1.** SDs ( $\text{g C m}^{-2} \text{ day}^{-1}$ ) of the prior flux uncertainties at country scale for July when considering  $B_{250}$  (a) and  $B_{150}$  (b). Red dots: ICOS66. Red/blue colors indicate relatively high/low uncertainties (with min =  $0 \text{ g C m}^{-2} \text{ day}^{-1}$ , max =  $1.975 \text{ g C m}^{-2} \text{ day}^{-1}$  in the color scale).

[Title Page](#)[Abstract](#)[Introduction](#)[Conclusions](#)[References](#)[Tables](#)[Figures](#)[◀](#)[▶](#)[◀](#)[▶](#)[Back](#)[Close](#)[Full Screen / Esc](#)[Printer-friendly Version](#)[Interactive Discussion](#)

## On the potential of ICOS atmospheric CO<sub>2</sub> measurement network

N. Kadygrov et al.

Title Page

Abstract

Introduction

Conclusions

References

Tables

Figures

◀

▶

◀

▶

Back

Close

Full Screen / Esc

Printer-friendly Version

Interactive Discussion

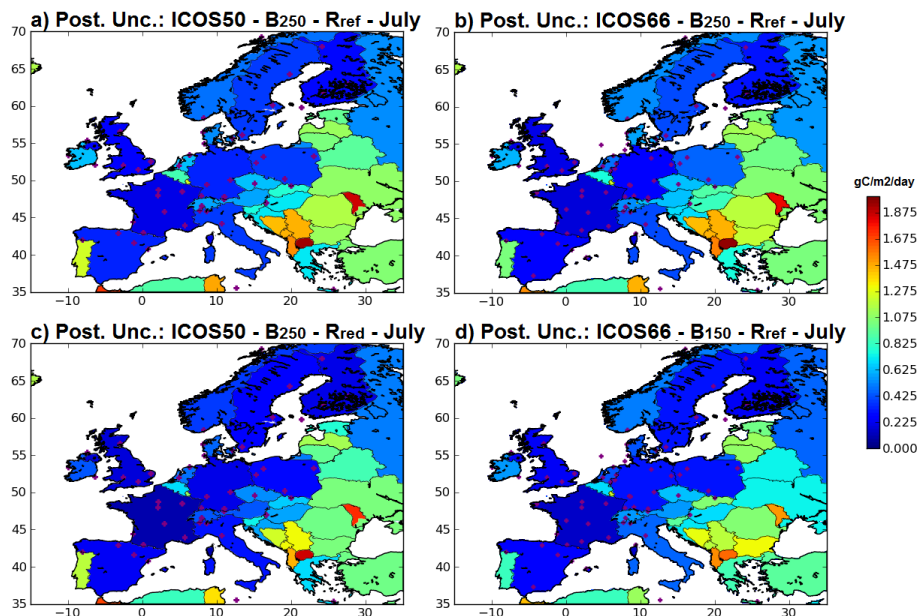


**Figure A2.** SDs ( $\text{gCm}^{-2}\text{day}^{-1}$ ) of the posterior uncertainties at country scale for July when using ICOS50 (**a**, **c**) and ICOS66 (**b**, **d**), the reference inversion configuration (**a**, **b**), using  $\mathbf{B}_{150}$  instead of  $\mathbf{B}_{250}$  (**d**) using  $\mathbf{R}_{\text{red}}$  instead of  $\mathbf{R}_{\text{ref}}$  (**c**). Red/blue colors indicate relatively high/low uncertainties (with min =  $0\text{gCm}^{-2}\text{day}^{-1}$ , max =  $1.975\text{gCm}^{-2}\text{day}^{-1}$  in the color scale).

## On the potential of ICOS atmospheric CO<sub>2</sub> measurement network

N. Kadygrov et al.

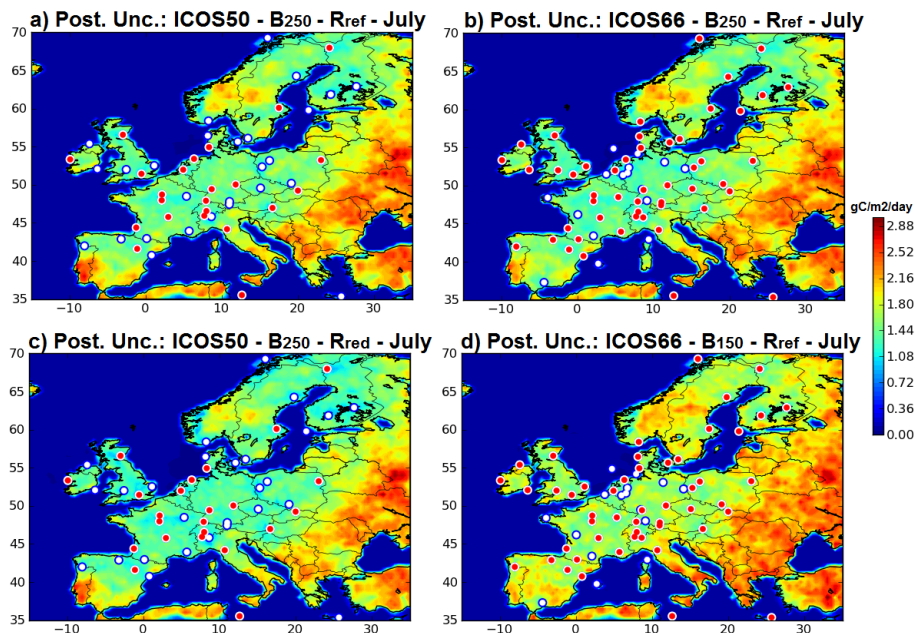


**Figure A3.** SDs ( $\text{gCm}^{-2}\text{day}^{-1}$ ) of the posterior uncertainties in two-week mean NEE at  $0.5^\circ$  resolution for July when using ICOS50 (**a, c**) and ICOS66 (**b, d**), the reference inversion configuration (**a, b**), using  $\mathbf{B}_{150}$  instead of  $\mathbf{B}_{250}$  (**d**) using  $\mathbf{R}_{\text{red}}$  instead of  $\mathbf{R}_{\text{ref}}$  (**c**). Red dots corresponds to the ICOS23 (**a, c**) or ICOS50 (**b, d**) sites while white dots correspond to the additional sites included in ICOS50 or ICOS66 respectively. Red/blue colors indicate relatively high/low uncertainties (with min =  $0\text{ gCm}^{-2}\text{day}^{-1}$ , max =  $3\text{ gCm}^{-2}\text{day}^{-1}$  in the color scale).

[Title Page](#)
[Abstract](#)
[Introduction](#)
[Conclusions](#)
[References](#)
[Tables](#)
[Figures](#)
[Back](#)
[Close](#)
[Full Screen / Esc](#)
[Printer-friendly Version](#)
[Interactive Discussion](#)